swiss physical society

Nr. 66, Januar 2022

SPG Mitteilungen
Communications de la SSP

Auszug - Extrait

Progress in Physics (89)

Hydrodynamics of fish swimming and mechanical regulation of regeneration

Christof M. Aegerter, Physik-Institut, Universität Zürich, Winterthurerstrasse 190, 8057 Zürich

Progress in Physics (89)

Hydrodynamics of fish swimming and mechanical regulation of regeneration

Christof M. Aegerter, Physik-Institut, Universität Zürich, Winterthurerstrasse 190, 8057 Zürich

1 Introduction

In development, organisms have to grow organs that are well adapted for their respective function, while at the same time being robust enough to cope with environmental variations [1 - 4]. Thus there are robust and stable genetic programs that are followed during development that lead to very similarly shaped organs even in the presence of changes in temperature or other such factors [5]. On the other hand functionally relevant environmental factors [6, 7] can have a profound influence on organ size and shape, such as in the liver or the bones of land animals, therefore necessitating a certain amount of plasticity in growth [8] and development [9, 10].

One such functionally relevant environmental factor is mechanical stress, which has long been known to lead to the development of bone shapes ideally suited for the incurred loads [11, 12]. This is known as Wolff's law in anatomy and for instance explains the different skeleton shapes observed in differently sized animals in the absence of a direct genetic prescription of bone shape. On another level, this law is used in Anthropology to infer the behavior of our ancestors from the found skeletons. In spite of its common application however, the biomechanical and genetic mechanisms behind Wolff's law remain mostly unknown.

Here we describe to use the zebrafish caudal fin as a model system to study the interplay between the environment and genetic regulation in the formation of shape and size in bone and organ development [6, 13]. This model system has several advantages that make a detailed study of the influence of mechanical forces on shape and size amenable. Being one of the modern model organisms, many genetic regulatory factors in growth control are known and genetic and biochemical tools for the manipulation of growth and development are available [5]. Furthermore, the fin is one of the very few vertebrate organs, which can fully regenerate. Therefore, the growth of the fin can be studied in two very distinct settings: as part of an organism that increases in size over time as well as part of a fully grown organism, where in both cases the overall function of propulsion is conserved. However, due to the change in Reynolds number in the two different settings, the type of swimming and therefore the ideal shape for propulsion, changes in the two situations [14, 15]. This indicates a second interest into the zebrafish fin, since its function and interaction with the environment is governed by hydrodynamics at intermediate Reynolds numbers, which is also a challenge experimentally as well as computationally. Here, I will describe experiments on three dimensional particle tracking velocimetry to study the spatio-temporally acting forces on fins during swimming. In particular, I will discuss the experimental setup and validation of the system as well as some findings in terms of fish propulsion as well as fin regeneration that we have been able to obtain in collaboration with biologists studying the process from a molecular point of view.

2 Experimental Setup and Data Analysis

In order to study the flow field around a deformable, flapping fin, we use three dimensional particle tracking velocimetry based on stereo imaging using three cameras [16, 17]. For an accurate determination of the flow speeds of the tracer particles, we use a double pulsed laser system for illumination, where the pulse separation δt between two adjacent pulses corresponds to the temporal distance between two snap shot of the three dimensional particle positions, hence giving rise to a determination of the velocity. By the combination of the three cameras, each frame consists effectively of triplets of particles forming a triangle, whose size and orientation determine the position in the depth of the field of view, which is defined as the z-direction below. Due to the shortness of the time interval δt, the separation of the par-

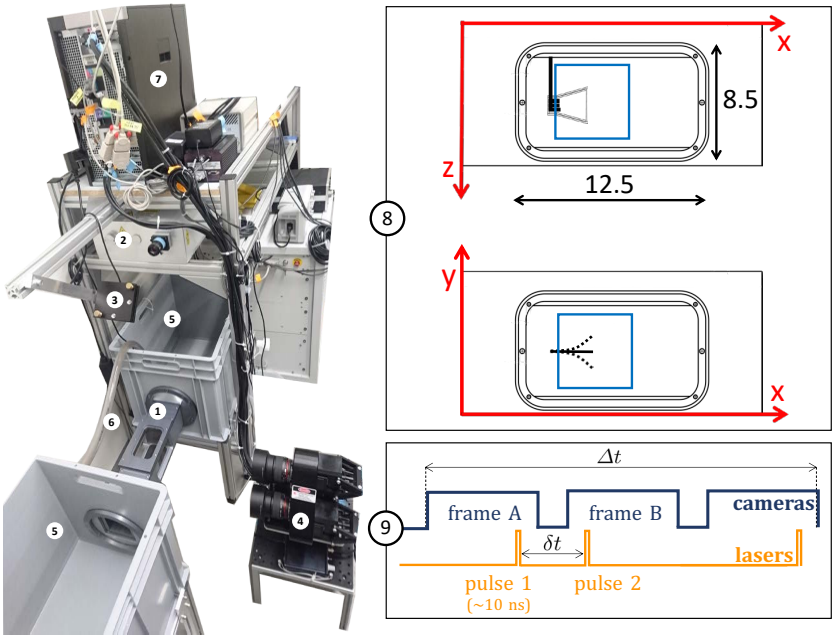

Figure 1: Experimental setup for 3D-3C PTV. (1) Flow chamber with transparent windows on three sides and a fixation wall on one side for inserting the synthetic fin. (2) Dual-head pulsed Nd:YAG laser with wave-length of 532 nm and maximal energy of 120 mJ/pulse, equipped with a pair of cylindrical lenses to expand the beam. (3) Mirror to deflect the laser beam. (4) Three cameras (resolution 4 MP, 85 mm lenses, sensor size 11.3 × 11.3 mm², magnification 0.3, maximal frequency of capture 180 Hz) mounted on a triangular plate parallel to the front wall of the flow chamber (x – y plane). The distance between the cameras plate and the center of the water tunnel is ≃ 465 mm. (5) Water tanks for the recirculating system. (6) Pipe and pump to control the flow. (7) V3V software and synchronizer. (8) Close-up of the flow chamber with inner dimensions (in cm), PTV-interrogation volume in blue (≃ 50 × 50 × 20 mm³) and sketch of the trapezoidal fin. Frontal view (x – y plane) and top view (x – z plane). (9) Frame straddling method with δt between the particle images and Δt between the velocity fields. Adapted from [18].

ticles has been small enough for a distinction of neighbour pairs to determine the velocity of the tracer particle in 3D. With a camera frame rate of 120 Hz, we thus obtain a full 3D flow field of the illuminated volume of 50 × 50 × 20 mm^3 at a time resolution of up to 60 Hz. With a spatial resolution of the particle positions of 3.6 μm in the *x*- and *y*-direction and 32 μm in the *z*-direction, the flow field is determined with an accuracy of 2 mm/s in the *x*- and *y*-directions and 18 mm/s in the *z*-direction [18]. From these velocity-fields we can then determine the hydrodynamic stresses via differentiation for the viscous stresses:

$$\tau_{ij} = \mu\left(\frac{\partial u_i}{\partial x_j} + \frac{\partial u_j}{\partial x_i}\right), \quad (1)$$

where μ is the dynamic viscosity and by integrating the pressure gradient given by the Navier-Stokes equation in terms of derivatives of the flow field by [19, 20]

$$\frac{\partial p}{\partial x_i} = -\rho\left(\frac{\partial u_i}{\partial t} + u_i\frac{\partial u_i}{\partial x_i} + u_j\frac{\partial u_i}{\partial x_j} + u_k\frac{\partial u_i}{\partial x_k}\right) + \mu\left(\frac{\partial u_i^2}{\partial x_i^2} + \frac{\partial u_i^2}{\partial x_j^2} + \frac{\partial u_i^2}{\partial x_k^2}\right), \quad (2)$$

where ρ is the density of the fluid. For this purpose, we use the queen2 algorithm, which is available at http://dabirilab.com/software/ [21].

Thus we are able to determine the full hydrodynamic stress tensor $\sigma_{ij} = -p\delta_{ij} + \tau_{ij}$ dependent on space and time. In addition, we are able to determine the position of the flapping fin from the absence of identified tracking particles, such that we can project the stress tensor onto the surfaces of the flapping fin and thus create spatio-temporally dependent force maps on the flapping fins. As a control of the accuracy of these force maps, integrating them along the width of the fin directly yields the force per unit length along the flexible fin, which is bent by these hydrodynamic forces. In addition, the shape of the bent fin is known from the experiment and its bending stiffness can be determined experimentally [22]. From this it is then possible to calculate the force per unit length acting on the fin based on the bending state using Euler-Bernoulli beam theory in order to calibrate the force determination from the hydrodynamic flows.

3 Calibration of the Method Using Euler-Bernoulli Beam Theory

Given a time dependent force acting on a flexible beam, its bending can be calculated using [23]

$$f_n(x,t) = m(x)\frac{\partial^2 h(x)}{\partial t^2} + \frac{\partial^2}{\partial x^2}\left(EI(x)\frac{\partial^2 h(x)}{\partial x^2}\right). \quad (3)$$

Here, *h(x)* is the midline position along the y-direction, f_n is the force per unit length along the x-direction varying temporally and $m(x) = \rho_f w(x) d$ and $EI(x) = E\frac{w(x)d^3}{12}$ are the mass per unit length and the bending stiffness respectively, where *w(x)* is the width of the fin. In the equation above, the first term on the right hand side describes the inertial force needed to displace the water surrounding the bent fin. The second term corresponds to the elastic force needed to bend the fin into the observe shape. In the most general case, one would also introduce viscous damping forces for both of these processes, however for the flapping frequencies and size of the fin we are studying here, these are negligible. In order to obtain a continuous description of the midline positions with only a few parameters, we fit the solution to a freely vibrating beam clamped at one end to the observed midlines.

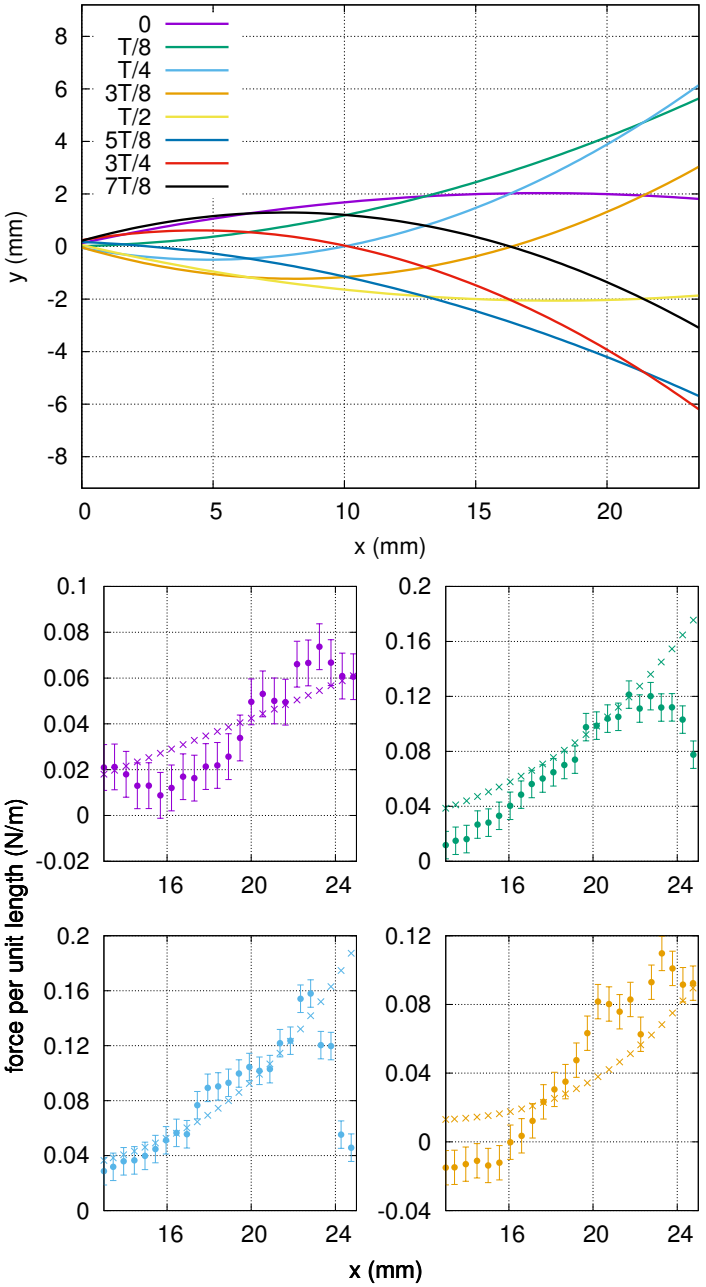

Figure 2: A: Foil midline positions at different time points during the oscillatory flapping. B: Force per unit length along the proximo-distal axis of the fin, from the PTV-based stress distributions (full circles) and the Euler-Bernoulli load calculation (crosses), at t0, t1/8, t1/4 and t3/8 from top left to bottom right, respectively. Adapted from [18].

The comparison of the results is shown in Fig. 2, which demonstrates that the determined forces per unit length capture the behaviour of the forces determined from beam theory quite well, except for the end tips of the fin, where the force drop is not reproduced by beam theory. At these positions however, fit capturing the curvature of the fins is not very accurate, such that the observed deviations are not surprising and we are confident that the hydrodynamic force maps present a more accurate physical picture. In addition, a control volume analysis [18] and a study of the vorticity in the fluid volume [24, 25] show that the forces determined

from the hydrodynamic flows can be used with an accuracy of about 0.01 to 0.02 N/m. Similarly, the viscous stresses are determined to an accuracy of a few mPa and the normal stresses to below 1 Pa. With such accurate measurements of force distributions on flapping fins, we can then study the effect of these forces during regeneration of zebrafish fins.

4 Hydrodynamic Forces during Fin Regeneration

In order to study the influence of hydrodynamic forces on fin regeneration, we have determined the influence of shape changes on growth rates in regeneration experiments in actual zebrafish fins [26]. Subsequently, we have determined the force maps on differently sized and shaped fins using particle tracking velocimetry as described above. Comparing the forces acting at different shapes and sizes with the growth rates of regenerating fins, we were then able to correlate the growth with certain components of the forces acting on the fin. Given that the growth takes place at the tip of the fin, we expected the forces at the outer edge of the fin to be the most promising candidates, which in a complete study of the stress tensor has shown to be the case, with only one component of the stress correlating with all the observational data on growth rates as a function of shape and size.

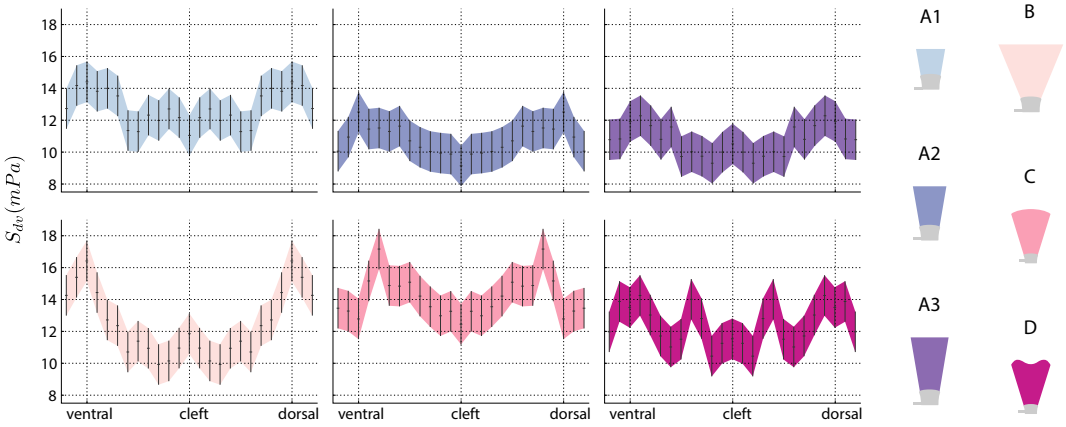

Figure 3: Spatial distribution of dorso-ventral shear stress at the tip of hydrofoils, $|S^t_{dv}|$. Shown is the dependence along the dorsoventral direction of the absolute value, averaged over a flapping period for differently sized and shaped fins. A growth promoting effect of this stress is consistent with growth termination at the correct size, different growth rates for fins of different width as well as the dependence of the depth of the cleft of the fin in fins of different width. Adapted from [26].

This candidate stress for growth control that we have been able to thus identify, consists of the shear stress along the dorsoventral direction in a fish fin. This corresponds to the *z*-direction of the experimental setup shown in Fig. 1. The period averages of the absolute values of this stress component are shown in Fig. 3 along the tip for six different fin shapes and sizes. Comparing fins A1 to A3 corresponding to an increase in length and hence mirroring growth of the fin, the results are consistent with a growth promotion of such a mechanical stress, leading to a deceleration of growth with increased length. In addition, experimental regeneration studies have shown that changing the width of the regrown fin by constant ablation leads to (i) decreased size with decreased width and (ii) decreased depth of the cleft of the fin (the indentation in the middle) with decreased width of the fin. Both of these structural features are also borne out by the force distributions shown in Fig. 3 for the differently shaped fins [26].

5 Conclusions and Outlook

Using three dimensional tracking of particles, it is possible to determine the full hydrodynamic forces acting on a flapping fin dependent on both space and time [18, 27–29]. Using proper control measurements and calibrations, we have shown that the thus determined values are a good representation of the forces acting on the fin.

The applications of such measurements of hydrodynamic forces can be used to study swimming efficiencies and propulsion mechanisms [30]. With these detailed measurements of forces acting on flapping fins, propulsion mechanisms and efficiencies for differently shaped fins can be weighed against each other. For instance, flapping frequency can counteract deficiencies in shape and thus lead to increased propulsion efficiency [24].

In addition, for small fish, where the flow regime is at intermediate Reynolds numbers [14], it is possible study the influence of boundary layer flows [19]. These can be important where spatial structures like ray bifurcations lead to different boundary layer flows and hence mixing of surface flows along the fish fin [31]. This can be sensed by the fish and leads to a more dense distribution of sensory cells in the tissue between bifurcated rays.

Above we have used this to study the influence of mechanical forces on the regeneration of zebrafish fins, where it is possible to find candidate stresses that act as growth regulators [26]. Hence, the regeneration can show phenotypic plasticity where the re-grown fin is adapted to the swimming forces acting on it, indicating a direct example of Wolff's law in a functional biological context. This information can now be used to guide studies of mechanisms of biological growth regulation on a molecular or genetic level and hence be used in the future for a mechanistic understanding of Wolff's law.

References

[1] G. Vogel, How do organs know when they have reached the right size? Science **340**, 1156-1157 (2013).
[2] C.-P. Heisenberg and Y. Bellaiche, Forces in tissue morphogenesis and patterning. Cell **153**, 948-962 (2013).
[3] A. Buchmann, M. Alber and J. J. Zartman, Sizing it up: the mechanical feedback hypothesis of organ growth regulation. Semin. Cell Dev. Biol. **35**, 73-81 (2014).
[4] V. Mwaffo, P. Zhang, S. Romero Cruz, M. Porfiri, Zebrafish swimming in the flow: A particle image velocimetry study, PeerJ **5,** e4041 (2017).
[5] D. Wehner and G. Weidinger, Signaling networks organizing regenerative growth of the zebrafish fin. Trends Genet. **31**, 336-343 (2015).
[6] P. E. Witten and B. K. Hall, Teleost skeletal plasticity: modulation, adaptation, and remodelling. Copeia **103**, 727-739 (2015).
[7] B. R. Aiello, M. W. Westneat and M. E. Hale, Mechanosensation is evolutionarily tuned to locomotor mechanics. Proc. Natl Acad. Sci. USA **114**, 4459 (2017).

[8] T. Aegerter-Wilmsen, C. M. Aegerter, E. Hafen and K. Basler, Model for the regulation of size in the wing imaginal disc of Drosophila. Mech. Dev. **124**, 318-326 (2007).
[9] D. E. Discher, D. J. Mooney, P. W. Zandstra, Growth factors, matrices, and forces combine and control stem cells., Science **324**, 1673 (2009).
[10] E. Frage, Mechanical induction of Twist in the Drosophila foregut/stomodeal primordium Curr. Biol. **13**, 1365 (2003).
[11] J. Wolff, *The Law of Bone Remodelling*. Berlin Heidelberg: Springer-Verlag (1986).
[12] F. A. Schulte, D. Ruffoni, F. M. Lambers, D. Christen, D. J. Webster, G. Kuhn and R. Müller, Local Mechanical Stimuli Regulate Bone Formation and Resorption in Mice at the Tissue Level. PLoS One **8**, e62172 (2013).
[13] A. P. Palstra, C. Tudorache, M. Rovira, S. A. Brittijn, E. Burgerhout, G. E. E. J. M. van den Thillart, H. P. Spaink, J. V. Planas, Establishing zebrafish as a novel exercise model: swimming economy, swimming-enhanced growth and muscle growth marker gene expression., PLoS One **5** (**12**) e14483 (2010).
[14] U. K. Müller, E. J. Stamhuis, J. J. Videler, Hydrodynamics of unsteady fish swimming and the effects of body size: Comparing the flow fields of fish larvae and adults, Journal of Experimental Biology **203**, 193—206 (2000).
[15] D. G. Sfakianakis, I. Leris, M. Kentouri, Effect of developmental temperature on swimming performance of zebrafish (danio rerio) juveniles, Environmental Biology of Fishes **90** (**4**) 421-427 (2011).
[16] F. J. A. Pereira, H. Stüer, E. C. Graff, M. Gharib, Two-frame 3d particle tracking. Measurement Science and Technology **17,** 1680 (2006).
[17] W. Lai, G. Pan, R. Menon, D. Troolin, E. Castaño-Graff, M. Gharib, F. J. A. Pereira, Volumetric three-component velocimetry: a new tool for 3d flow measurement. In *14th Int. Symp. on Applications of laser Techniques to Fluid Mechanics* (2008).
[18] P. Dagenais, C. M. Aegerter, Hydrodynamic stress maps on the surface of a flexible fin-like foil. PLoS ONE **16**(**1**) e0244674 (2021).
[19] L. Prandtl, *Essentials of fluid dynamics: With applications to hydraulics, aeronautics, meteorology, and other subjects*, (1952) (various printings), Hafner Pub. Co., (1952).
[20] G. K. Batchelor, *An Introduction to Fluid Dynamics*, Cambridge Mathematical Library, Cambridge University Press, (2000).
[21] J. O. Dabiri, S. Bose, B. Gemmell, S. Colin, J. Costello, An algorithm to estimate unsteady and quasi-steady pressure fields from velocity field measurements, The Journal of Experimental Biology **217,** 331-36 (2014).
[22] S. Puri, T. Aegerter-Wilmsen, A. Jazwinska, C. M. Aegerter, In vivo quantification of mechanical properties of caudal fins in adult zebrafish, Journal of Experimental Biology **221** (**4**), 17077 (2018).
[23] F. Paraz, L. Schouveiler, C. Eloy, Thrust generation by a heaving flexible foil: Resonance, nonlinearities, and optimality, Physics of Fluids **28,** 011903 (2016).
[24] P. Dagenais, C. M. Aegerter, How shape and flapping rate affect the distribution of fluid forces on flexible hydrofoils. Journal of Fluid Mechanics **901**, A1 (2020).
[25] T. Schnipper, A. Andersen, T. Bohr, Vortex wakes of a flapping foil, Journal of Fluid Mechanics **633,** 411-423 (2009).
[26] P. Dagenais, S. Blanchoud, D. Pury, C. Pfefferli, T. Aegerter-Wilmsen, C. M. Aegerter, A. Jazwinska, Hydrodynamic stress and phenotypic plasticity of the zebrafish regenerating fin. Journal of Experimental Biology **224**, jeb242309 (2021).
[27] E. D. Tytell, E. M. Standen, G. V. Lauder, Escaping flatland: three-dimensional kinematics and hydrodynamics of median fins in fishes, Journal of Experimental Biology **211** (**2**) 187-195 (2008).
[28] B. E. Flammang, G. V. Lauder, D. Troolin, T. E. Strand, Volumetric imaging of fish locomotion, Biology Letters **7**, 695-8 (2011).
[29] R. Gurka, A. Liberzon, D. Hefetz, D. Rubinstein, U. Shavit, Computation of pressure distribution using piv velocity data, in: *Third Int. Work. PIV, Santa Barbara, CA, 1999*, 671-676.
[30] G. V. Lauder, P. G. A. Madden, Fish locomotion: Kinematics and hydrodynamics of flexible foil-like fins, Experiments in Fluids **43**, 641-653 (2007).
[31] D. König, P. Dagenais, A. Senk, V. Djonov, C. M. Aegerter, and A. Jazwinska, Distribution and restoration of serotonin-immunoreactive paraneuronal cells during caudal fin regeneration in zebrafish. Frontiers in Molecular Neuroscience **12**, 227 (2019).